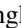










Magnetoelastic coupling driven magnon gap in a honeycomb antiferromagnet

Jeongheon Choe ^{1,2,*} Andrey Baydin ^{3,4,*} Gaihua Ye,^{5,*} Bowen Ma,¹ Cynthia Nnokwe,⁵ Martin Rodriguez-Vega ^{1,2,6}
 David Lujan,^{1,2} Swati Chaudhary,^{1,2,6} Fuyang Tay ^{3,7} Jiaming He ⁸ Hiroyuki Nojiri,⁹ Jianshi Zhou ^{2,8}
 Gregory A. Fiete ^{6,10} Junichiro Kono,^{3,4,11,12} Rui He ^{5,†} and Xiaoqin Li ^{1,2,‡}

¹*Department of Physics, Center of Complex Quantum Systems, The University of Texas at Austin, Austin, Texas 78712, USA*

²*Center for Dynamics and Control of Materials, The University of Texas at Austin, Austin, Texas 78712, USA*

³*Department of Electrical and Computer Engineering, Rice University, Houston, Texas 77005, USA*

⁴*Smalley–Curl Institute, Rice University, Houston, Texas 77005, USA*

⁵*Department of Electrical and Computer Engineering, Texas Tech University, Lubbock, Texas 79409, USA*

⁶*Department of Physics, Northeastern University, Boston, Massachusetts 02115, USA*

⁷*Applied Physics Graduate Program, Smalley–Curl Institute, Rice University, Houston, Texas 77005, USA*

⁸*Department of Mechanical Engineering, The University of Texas at Austin, Austin, Texas 78712, USA*

⁹*Institute for Materials Research, Tohoku University, Sendai 980-8577, Japan*

¹⁰*Department of Physics, Massachusetts Institute of Technology, Cambridge, Massachusetts 02139, USA*

¹¹*Department of Physics and Astronomy, Rice University, Houston, Texas 77005, USA*

¹²*Department of Materials Science and NanoEngineering, Rice University, Houston, Texas 77005, USA*



(Received 10 May 2023; revised 26 August 2024; accepted 28 August 2024; published 13 September 2024)

Cobalt titanate, CoTiO_3 , is a honeycomb antiferromagnet recently confirmed experimentally to host Dirac magnons, topological spin-orbit excitons, and chiral phonons. Here, we investigate a magnon gap at the zone center which calls for a refined spin Hamiltonian. We propose a microscopic model for the magnon gap and attribute it to a lattice-distortion (phonon)-induced higher-order spin interaction. Strong magnetoelastic coupling in CoTiO_3 is also evident in Raman spectra, in which the magnetic order exerts a stronger influence on phonons corresponding to in-plane ionic motions than those with out-of-plane motions. We further examine the evolution of the zone-center magnons in a high magnetic field up to 18.5 T via THz absorption spectroscopy measurements. Based on this field dependence, we propose a spin Hamiltonian that not only agrees with magnon dispersion measured by inelastic neutron scattering but also includes fewer exchange constants and a realistic anisotropy term. Our work highlights the broad implications of magnetoelastic coupling in the study of topologically protected bosonic excitations.

DOI: [10.1103/PhysRevB.110.104419](https://doi.org/10.1103/PhysRevB.110.104419)

I. INTRODUCTION

Many exotic properties have been predicted in honeycomb magnets with spin-orbit coupling. Some of these phenomena, such as spin-momentum locking, counter-rotating spin spirals, and unusual thermal Hall effects, have been observed in $5d$ and $4d$ compounds such as iridates and related materials, e.g., RuCl_3 [1–3]. While theoretical studies are typically based on a model Hamiltonian in which one type of spin interaction, e.g., Kitaev interaction, dominates, spin Hamiltonians for realistic materials usually include more terms to account for complex interactions between spins. The search for quantum and topological spin states has recently expanded to $3d$ Co^{+2} compounds. In particular, CoTiO_3 (CTO) has been found to be a particularly interesting material that hosts Dirac magnons [4,5], chiral phonons [6,7], and topological spin-orbit excitons [5,8].

An intricate interplay between charge, spin, orbital, and lattice degrees of freedom is generally anticipated in correlated materials. In CoTiO_3 , a large magnetic moment or chirality associated with phonons has been observed and attributed to the coupling between phonons and spin-orbit excitons that are in close proximity energetically [6,7]. As another example, spin-spin correlations have been found to cause abrupt changes in the dielectric permittivity and heat capacity across the Néel temperature [9–11]. Furthermore, hybridization between magnons and phonons has been predicted to lead to nontrivial band topology and, consequently, a thermal Hall effect [12–16]. Several of these prior observations originate from magnetoelastic coupling, which affects magnon spectra in the leading order. Because magnetoelastic coupling does not require broken inversion symmetry of the bonds, it is more widely present than other spin interactions, e.g., the extensively studied Dzyaloshinskii-Moriya interaction [17–19]. In general, interactions that break a continuous spin rotational symmetry are predicted to lead to a magnon gap at the Brillouin zone center, which places important constraints on magnon dynamics, and/or near the Dirac points, which is critical for topological protection.

*These authors contributed equally to this work.

†Contact author: rui.he@ttu.edu

‡Contact author: elaineli@physics.utexas.edu

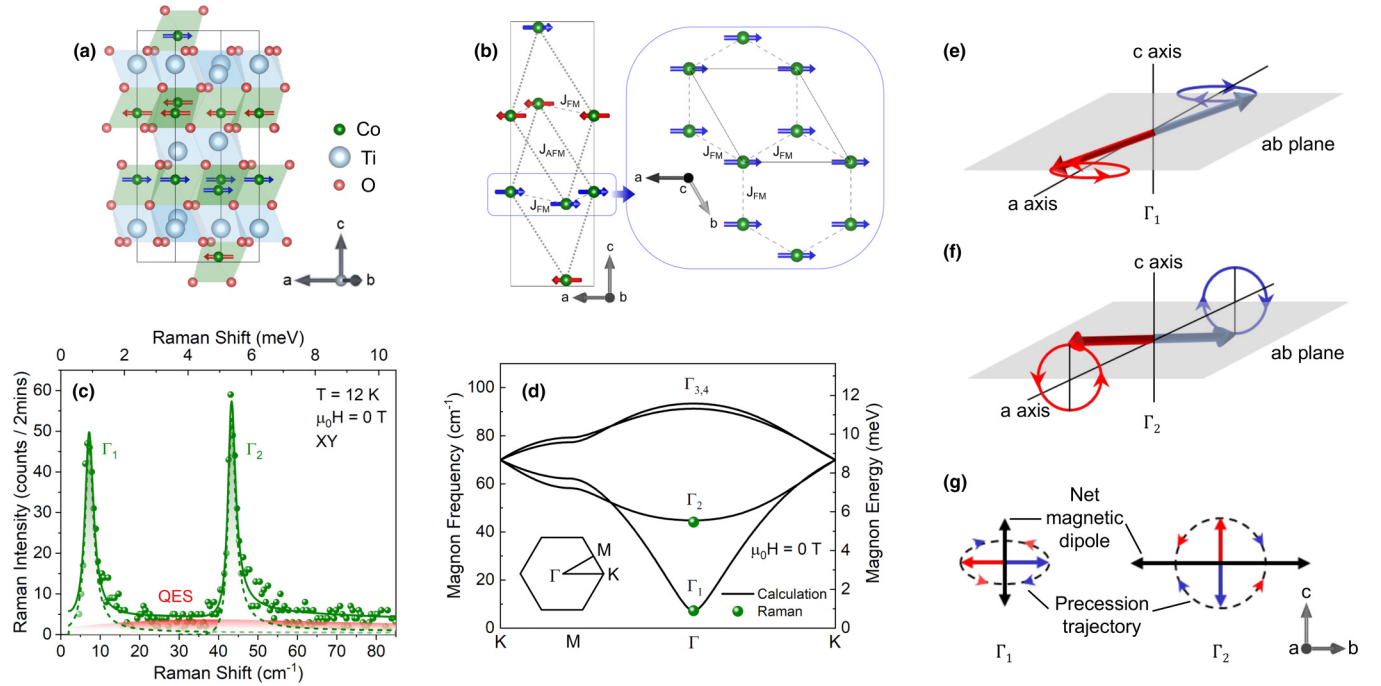


FIG. 1. AFM magnons in CoTiO_3 . (a) Crystal structure. (b) Magnetic configuration in the AFM phase. The Co^{2+} magnetic moments (blue and red arrows) are ferromagnetically (antiferromagnetically) ordered within (perpendicular to) the ab plane. The left (right) panel represents a side (top) view of stacked honeycomb layers. The black solid lines show the magnetic unit cell. (c) Raman spectrum taken at 12 K at zero field in the XY polarized channel. Green dashed curves are Fano function fits. The red-shaded region represents the fitting of the quasielastic scattering (QES) peak. Green solid curves are cumulative fits. (d) Calculated magnon dispersion at zero field. The green dots are measured data from Raman scattering. The inset represents high-symmetry points in the magnetic Brillouin zone. Schematic of (e) Γ_1 and (f) Γ_2 magnon precession around the a axis are elliptical and circular, respectively. Red and blue arrows indicate magnetic moments whose directions are opposite in adjacent honeycomb layers (ab plane). (g) The sum of the oscillating magnetic moments corresponds to the magnetic dipole direction shown as black arrows.

Here, we report the observation of a zone-center magnon gap in CTO in Raman spectra and attribute it to magnetoelastic coupling. The presence of strong magnetoelastic coupling is corroborated by the temperature dependence of the E_g phonon mode, in which the in-plane Co^{2+} magnetic ion displacement modulates the strong ab -plane exchange interactions. In contrast, the A_g mode corresponding to out-of-plane atomic vibrations exhibits a weaker spin-lattice coupling. Microscopically, we describe this lattice-distortion-induced higher-order spin interaction by a quartic spin interaction term that arises from the coupling of the elastic strain tensor to spin bilinears. Furthermore, we study how zone-center magnons evolve in high magnetic fields up to 18.5 T using terahertz (THz) absorption spectroscopy. Based on this field dependence, we propose a refined XY+XXZ spin Hamiltonian for CTO. This Hamiltonian not only includes a significantly reduced number of exchange parameters and a more realistic anisotropic interlayer coupling compared to other proposed Hamiltonians, it also reproduces magnon energy at a much higher B field inaccessible in previous studies. By clarifying the microscopic origin of the magnon gap and refining the spin Hamiltonian, our study guides the search for $3d$ Co^{+2} compounds, in addition to previously studied quaternary compounds [e.g., $\text{BaCo}_2(\text{AsO}_4)_2$], for exploring interesting topological phenomena associated with bosons.

II. RESULTS AND DISCUSSION

CTO crystallizes in the ilmenite structure ($R\bar{3}$), composed of edge-sharing CoO_6 and TiO_6 octahedra layers, alternately stacked along the c axis [Fig. 1(a)]. CTO is an A -type antiferromagnet (AFM) with Néel temperature $T_N = 38$ K. The magnetic structure consists of buckled two-dimensional (2D) honeycomb lattices of Co^{2+} ions in the ab plane and an ABC -stacking sequence along the c axis. Nearest-neighbor Co^{2+} ions in the quasi-2D layers are ferromagnetically coupled with exchange constant J_{FM} whereas ions in adjacent layers are antiferromagnetically coupled with exchange constant J_{AFM} [Fig. 1(b)]. Within each layer, there are two magnetic sublattices associated with the hexagonal lattice. In a magnetic primitive unit cell, there are four magnetic sublattices of Co^{2+} ions. Thus, four magnon branches are expected and plotted in the calculated magnon dispersion shown in Fig. 1(d).

We perform Raman scattering experiments in the backscattering geometry where the incident light propagates along the a axis, perpendicular to the surface of CTO crystal. At $T = 12$ K with no applied magnetic field, Raman spectroscopy revealed two zone-centered magnon modes, Γ_1 and Γ_2 , with cross-linearly polarized incident and scattered light (i.e., XY channel), as shown in Fig. 1(c). All Raman spectra are taken

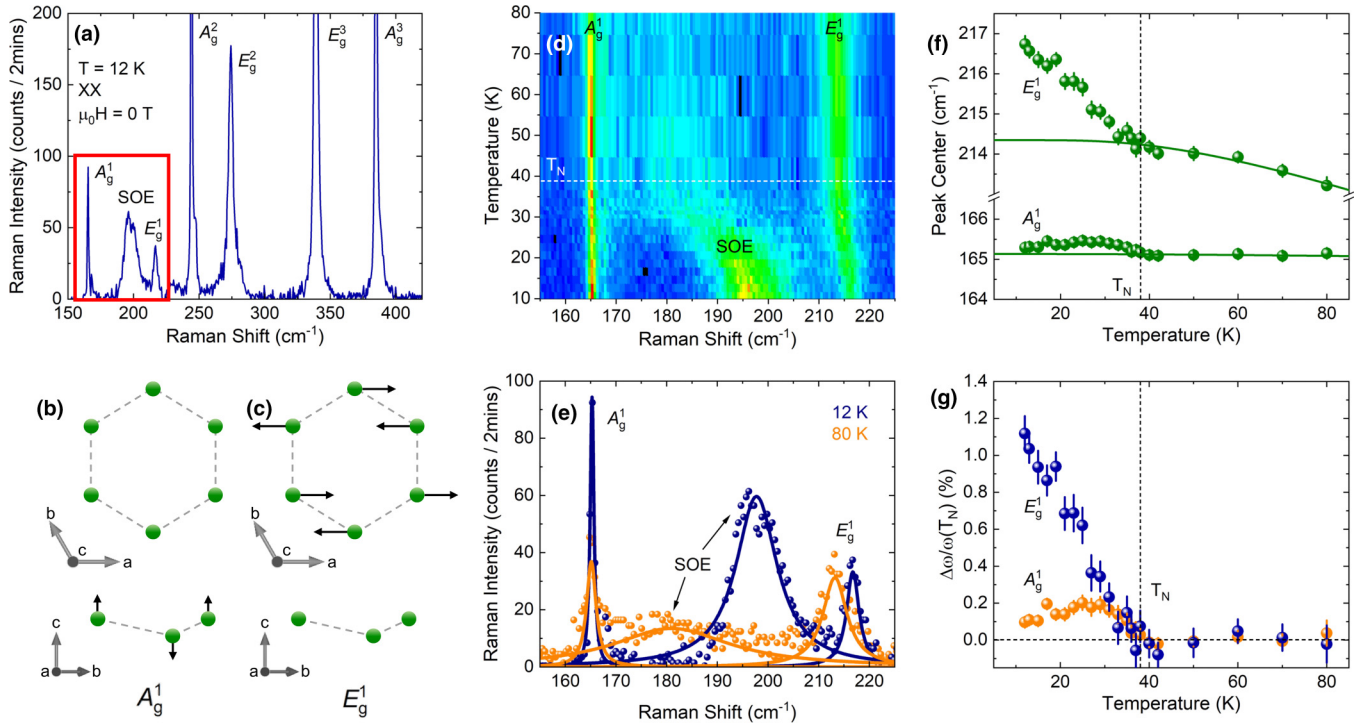


FIG. 2. Magnetoelastic coupling signatures observed in Raman spectra. (a) Raman spectra measured at 12 K at zero field. Enclosed in the red box are A_g , E_g phonon modes and spin-orbit exciton (SOE), respectively. Top and side view of atomic displacement of Co^{2+} ions in (b) A_g^1 and (c) E_g^1 phonon mode. (d) Temperature-dependent spectra of A_g^1 , SOE, and E_g^1 . (e) Raman spectra taken at 12 and 80 K. Points are data, while solid lines are Lorentzian fits. (f) Central frequencies of A_g^1 and E_g^1 modes as a function of temperature. Solid curves are fits by an anharmonic phonon-phonon interaction model. (g) Relative Raman shift of A_g^1 and E_g^1 after subtracting the fitting curves based on the anharmonic model.

with a 532-nm laser unless otherwise stated. We attribute the observed asymmetric magnon line shape to interference with a quasielastic scattering (QES) peak due to spin fluctuations (more details in the Supplemental Material [20]).

Visualizing the magnetic moment precession informs the coupling between a magnon mode and light. We calculate the eigenvector of Γ_1 and Γ_2 magnon modes based on the XXZ Hamiltonian with anisotropic exchange coupling and obtain the relative phase of spin precession of magnetic sublattices in adjacent layers. The magnetic moment precessions of the Γ_1 and Γ_2 modes observed in the AFM phase are illustrated in Figs. 1(e) and 1(f), respectively. For the Γ_1 magnon mode, the precession of magnetic moments is highly elliptical due to the easy-plane anisotropy, which has a smaller out-of-plane component than the Γ_2 magnon. Magnetic moments in adjacent layers (red and blue arrows) are opposite to each other. The out-of-plane component of the magnetic moment precesses in phase and out of phase for the Γ_1 and Γ_2 magnon modes, respectively. The net magnetic moment of the Γ_1 (Γ_2) mode oscillates along the c axis (within the ab plane) as illustrated in Fig. 1(g).

We identify signatures of coupling between spin, lattice, and orbital degrees of freedom in Raman spectra in a higher-energy range than the zone-center magnons (Fig. 2). We focus on two phonon modes A_g , E_g , and a spin-orbit exciton (SOE), enclosed in the red box in Fig. 2(a). These mode assignments are consistent with earlier Raman and inelastic neutron scattering (INS) measurements [5,8,11]. SOEs are also known as

orbital waves, and they correspond to electronic excitations between Kramers doublets in Co^{2+} $3d$ orbitals. SOEs couple to phonons directly due to partial spectral overlap [6] and to magnons only indirectly.

Magnetoelastic coupling, or spin-lattice coupling, can be quantified via temperature-dependent phonon frequencies. Temperature-dependent Raman spectra for the A_g^1 , SOE, and E_g^1 modes are shown in Figs. 2(d)–2(f). As an example, spectra taken at 12 and 80 K are shown in Fig. 2(e). The central frequencies of the A_g^1 and E_g^1 mode extracted from Lorentzian fittings (solid lines) are summarized in Fig. 2(f). Above T_N [paramagnetic (PM) phase], the phonon frequencies follow an anharmonic phonon-phonon interaction model (the solid fitting lines), $\omega(T) = \omega_0 - A[1 + 2n(\omega/2, T)]$, where ω_0 is the bare phonon frequency, A is the phonon-phonon scattering strength, and n is the phonon population calculated with the Bose-Einstein distribution. Below T_N (AFM phase), the E_g^1 phonon frequency exhibits a larger deviation from the model than the A_g^1 mode, indicating stronger spin-lattice coupling. This difference is expected. For the E_g^1 (A_g^1) mode, in-plane (out-of-plane) motions of Co^{2+} ions directly modulate the intralayer (interlayer) exchange constant J_{FM} (J_{AFM}), where J_{FM} is much largely modulated than J_{AFM} . The spin-orbit-lattice coupling also dynamically modulates spins and leads to spin fluctuations, as manifested in the magnon Fano line shape in Fig. 1(c) due to interference with the QES peak (more details in the Supplemental Material [20] and Refs. [21–26] therein).

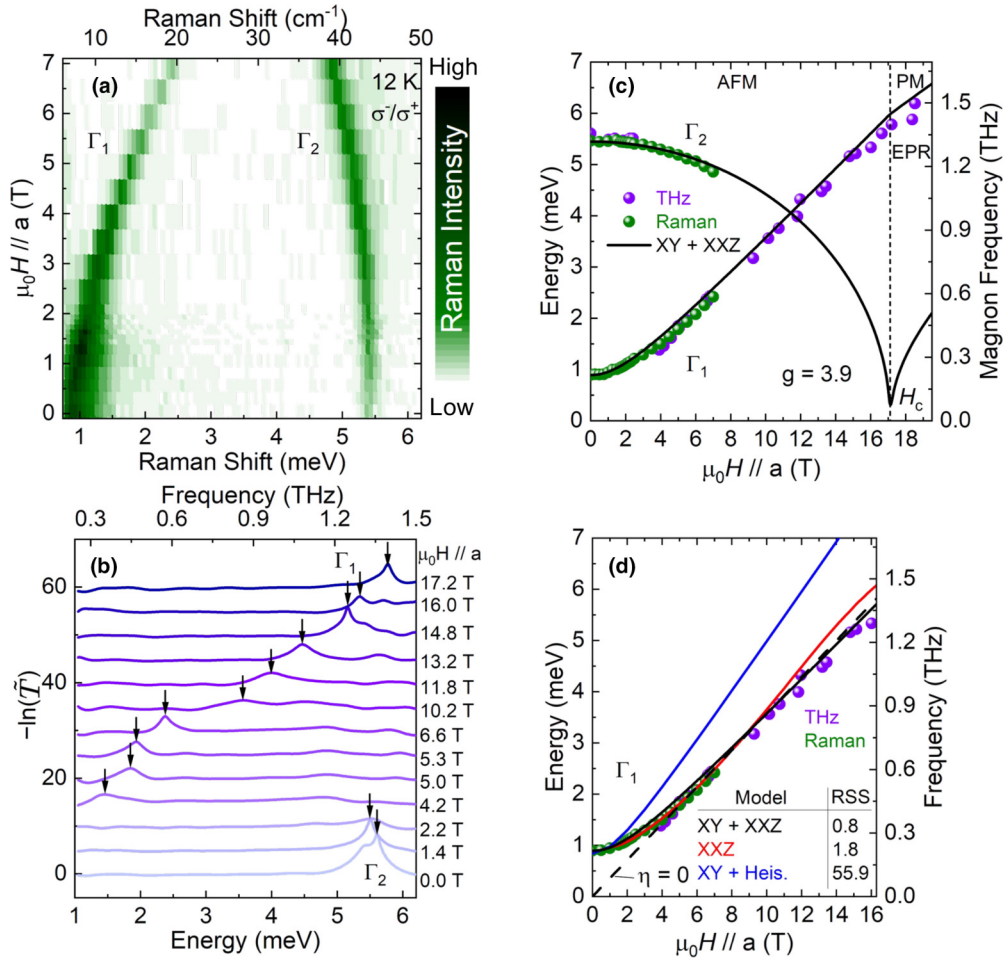


FIG. 3. Magnetic field dependence of the zone-center magnons in CTO. (a) Raman spectra taken with the cross-circular (σ^-/σ^+) polarized incident and scattered light at 12 K as a function of applied magnetic field. (b) THz absorption spectra, vertically offset for clarity, where \bar{T} is defined in the text. The arrows represent absorption peak centers. (c), (d) Magnon energies as a function of magnetic field along the a axis. Green (purple) dots are the magnon energies extracted from Raman (THz absorption) measurements. The fitting errors are smaller than the dot size. The critical field H_c represents the transition from the AFM phase to the PM phase. In (d), the residual sum of squares (RSS) is the sum of the squares of the difference between measured and calculated energies for a few models. Solid lines in (c) and (d) are fitting curves with a detailed explanation in the text.

To assess the strength of magnetoelastic coupling in CTO and compare it with other materials, we plot the relative frequency shift, $\Delta\omega/\omega(T_N) = [\omega(T) - \omega(T_N)]/\omega(T_N)$, as a function of T ; see Fig. 2(g). Below $\omega(T_N)$, the frequency of the E_g^1 mode monotonically increases, reaching $\sim 1.1\%$ at the lowest temperature. This value is comparable to that in $\text{Cr}_2\text{Ge}_2\text{Te}_6$ ($\sim 1\%$), Fe_3GeTe_2 ($\sim 0.7\%$), MnBi_2Te_4 ($\sim 0.3\%$), and FePS_3 ($\sim 0.2\%$) [26–29] due to the strong spin-orbit coupling in these compounds.

Microscopically, the spin-lattice coupling originates from lattice-deformation-induced symmetry breaking. The $U(1)$ spin rotational symmetry is broken in a distorted 2D lattice, i.e., the ab plane containing Co atoms, leading to the zone-center magnon gap [30–33]. After a derivation outlined in detail in the Supplemental Material [20] (see also Refs. [30–38] therein), we obtain an effective lattice-distortion-induced quartic spin Hamiltonian [Eq. (9) in Supplemental Material [20]]. Employing linear spin-wave theory with the magnetic moments along the y axis then leads to the effective Hamiltonian $H_s \approx \sum_{i,\delta} \eta[(S_i^y)^2 + (S_{i+\delta}^x)^2 -$

$S_i^y S_{i+\delta}^y]$, with $\eta > 0$. We estimate $\eta = 24 \mu\text{eV}$ (see Supplemental Material [20]), which leads to a Γ -point magnon gap of $\Delta = 0.9 \text{ meV}$, close to the measured magnon gap. The quartic spin interaction is similar to the spin-lattice interaction studied in pyrochlore systems [30–32]. While the magnon gap in pyrochlore lattices is primarily attributed to a six-spin interaction term owing to the perfect cubic symmetry [33], CTO crystals experience trigonal distortion.

While magnetoelastic coupling determines the zone-center magnon energy at zero applied magnetic field, exchange coupling constants determine how the zone-center magnon frequencies shift with an applied magnetic field \vec{H} . In an AFM such as CTO, this field-dependent magnon frequency shift is small for fields less than 2 T; see Fig. 3(a). We extended Raman and THz absorption measurements to higher fields, as shown in Fig. 3. All measurements were performed at $T = 12 \text{ K}$ in external magnetic field \vec{H} applied along the a axis. Figure 3(a) shows Raman spectra taken in the crossed-circular polarization configuration (σ^-/σ^+) with a 532-nm laser. The Γ_1 magnon frequency increases

while the Γ_2 mode softens with increasing magnetic field. THz absorption spectra at various magnetic fields up to 17.2 T are shown in Fig. 3(b). The measurements were performed with the THz magnetic field along the c axis. We note that Γ_2 magnons are observed using a different THz magnetic field direction, likely due to the presence of multiple domains in the sample [10,39,40]. Here, the quantity $-\ln \tilde{T}(\omega, H)$ is plotted as a function of frequency ω for various H , where $\tilde{T}(\omega, H) = |\tilde{E}(\omega, 12.5 \text{ K}, H)/\tilde{E}(\omega, 50 \text{ K}, H = 0)|^2$ and $\tilde{E}(\omega, T, H)$ is the Fourier transform of the collected electric field waveforms. The data were taken using a THz time-domain magnetospectroscopy system [41] with a table-top pulsed magnet [42]. Both the Γ_1 and Γ_2 magnons are observed, and their magnetic-field-dependent frequencies are consistent with those observed in magneto-Raman spectroscopy. The Γ_1 magnon should be observable [40,43] at all fields, but its frequency falls outside the detection range of our THz setup when $\mu_0 H < 4 \text{ T}$. In contrast, the Γ_2 magnon mode is observable at low fields but disappears at high fields, likely due to spin-reorientation process around 2 T [10,39].

Figure 3(c) summarizes magnon energies extracted from both Raman (green circles) and THz (purple circles) measurements as a function of magnetic field from 0 to 18.5 T. In the PM phase ($\mu_0 H > \mu_0 H_c \sim 17 \text{ T}$), we assign the THz absorption peak to the electron paramagnetic resonance (EPR), only found in the PM phase [Fig. 3(c)]. In the absence of long-range magnetic ordering, the EPR is the excitation of exchange-coupled Co^{2+} ions' pseudospin states with $S = \pm 1/2$, where the EPR energy increases linearly with the external magnetic field.

To explain the magnetic-field-dependent Γ_1 magnon energy in the AFM phase as well as the EPR energy in the PM phase, we propose a modified XY+XXZ spin Hamiltonian, $\mathcal{H} = \sum_{i,\delta} \{J_\delta^\perp (S_i^x S_{i+\delta}^x + S_i^y S_{i+\delta}^y) + J_\delta^z S_i^z S_{i+\delta}^z\}$ with intralayer exchange coupling $\delta = \text{FM}$, interlayer coupling $\delta = \text{AFM}$ between neighboring i th and $i + \delta$ th Co^{2+} ion sites, $J_{\text{FM}}^\perp = -4.44$, $J_{\text{FM}}^z = 0$, $J_{\text{AFM}}^\perp = 0.65$, and $J_{\text{AFM}}^z = 0.3$ in units of meV, and $g = 3.9$. The XY+XXZ Hamiltonian itself yields a gapless Goldstone mode at zero magnetic field [black dashed curve in Fig. 3(d)]. The magnetoelastic coupling term H_s with $\eta = 24 \mu\text{eV}$ is added to the spin Hamiltonian to capture the magnon modes at low fields. The resulting fit based on our modified XY+XXZ spin Hamiltonian is shown by the black solid curves in Figs. 3(c) and 3(d).

We compare our XY+XXZ model with other spin Hamiltonians used in previous studies of CTO. In INS studies, two alternative spin Hamiltonians have been proposed: the XY+Heisenberg model [4] and the XXZ model [5,43]; see Fig. 3(d) and Supplemental Material [20]. These models cannot be distinguished by the magnon energy at zero magnetic field. However, in the presence of a magnetic field greater than 1 T applied along the a axis, the observed Γ_1 magnon energy starts to deviate from the XY+Heisenberg model given in Ref. [4], while the XXZ model from Refs. [5,43] fits the

field-dependent magnon energy well up to about 7 T. In the higher-field regime between 7 and 16 T, the magnon energy is best described by our modified XY+XXZ model as shown by the residual sum of squares (RSS) of the three spin models. We also calculated the magnon dispersion using the XY+XXZ model and found an excellent agreement with previous INS experiments [5] shown in the Supplemental Material [20].

III. SUMMARY

In summary, we studied CTO using two complementary optical spectroscopy methods, which primarily probe zone-center magnons. We not only measured the zone-center magnon gap accurately but also proposed a simple mechanism, magnetoelastic coupling, for the gap formation supported by phonon temperature dependence and quasielastic scattering peak analyses. Microscopically, a lattice-distortion-induced higher-order spin interaction leads to symmetry-lowering magnetic exchange anisotropy and modifies exchange constants. By extending both Raman and THz absorption measurements to higher magnetic fields, we proposed a refined spin Hamiltonian for CTO with fewer exchange parameters and a reasonable anisotropy term. While experiments presented here are static in nature, they may guide future ultrafast experiments in which phonons or magnons are coherently driven out of equilibrium to disentangle them or tune their coupling dynamically [44,45].

ACKNOWLEDGMENTS

This research was primarily supported by the National Science Foundation through the Center for Dynamics and Control of Materials: an NSF MRSEC under Cooperative Agreements No. DMR-1720595 and No. DMR-2308817. Additional support from NSF DMR-2114825 (for laser stimulation theory), DOE Award No. DE-SC0022168 (for magnetic anisotropy theory), and the Alexander von Humboldt Foundation is gratefully acknowledged by G.A.F. Support from Welch Foundation Chair F-0014 and NSF EPM program Grant No. DMR-2225645 is gratefully acknowledged by X.L. This work was performed in part at the Aspen Center for Physics, which is supported by National Science Foundation Grant No. PHY-1607611. G.Y., C.N., and R.H. acknowledge support by the National Science Foundation Grants No. DMR-2104036 and No. DMR-2300640. Parts of the experiments were performed at the user facility supported by the National Science Foundation through the Center for Dynamics and Control of Material under Cooperative Agreement No. DMR-1720595 and The Major Research Instrumentation (MRI) Program No. DMR-2019130. A.B., F.T., and J.K. acknowledges support from the U.S. Army Research Office (through Award No. W911NF2110157), the Gordon and Betty Moore Foundation (through Grant No. 11520), and the Robert A. Welch Foundation (through Grant No. C-1509).

[1] S. Hwan Chun, J.-W. Kim, J. Kim, H. Zheng, C. C. Stoumpos, C. Malliakas, J. Mitchell, K. Mehlawat, Y. Singh, Y. Choi *et al.*,

Direct evidence for dominant bond-directional interactions in a honeycomb lattice iridate Na_2IrO_3 , *Nat. Phys.* **11**, 462 (2015).

- [2] S. M. Winter, Y. Li, H. O. Jeschke, and R. Valentí, Challenges in design of Kitaev materials: Magnetic interactions from competing energy scales, *Phys. Rev. B* **93**, 214431 (2016).
- [3] Y. Kasahara, T. Ohnishi, Y. Mizukami, O. Tanaka, S. Ma, K. Sugii, N. Kurita, H. Tanaka, J. Nasu, Y. Motome *et al.*, Majorana quantization and half-integer thermal quantum Hall effect in a Kitaev spin liquid, *Nature (London)* **559**, 227 (2018).
- [4] B. Yuan, I. Khait, G.-J. Shu, F. C. Chou, M. B. Stone, J. P. Clancy, A. Paramakanti, and Y.-J. Kim, Dirac magnons in a honeycomb lattice quantum XY magnet CoTiO₃, *Phys. Rev. X* **10**, 011062 (2020).
- [5] M. Elliot, P. A. McClarty, D. Prabhakaran, R. D. Johnson, H. C. Walker, P. Manuel, and R. Coldea, Order-by-disorder from bond-dependent exchange and intensity signature of nodal quasiparticles in a honeycomb cobaltate, *Nat. Commun.* **12**, 3936 (2021).
- [6] D. Lujan, J. Choe, S. Chaudhary, G. Ye, C. Nnokwe, M. Rodriguez-Vega, J. He, F. Y. Gao, T. N. Nunley, E. Baldini *et al.*, Spin-orbit exciton-induced phonon chirality in a quantum magnet, *Proc. Natl. Acad. Sci. USA* **121**, e2304360121 (2024).
- [7] S. Chaudhary, D. M. Juraschek, M. Rodriguez-Vega, and G. A. Fiete, Giant effective magnetic moments of chiral phonons from orbit-lattice coupling, *Phys. Rev. B* **110**, 094401 (2024).
- [8] B. Yuan, M. B. Stone, G.-J. Shu, F. C. Chou, X. Rao, J. P. Clancy, and Y.-J. Kim, Spin-orbit exciton in a honeycomb lattice magnet CoTiO₃: Revealing a link between magnetism in *d*- and *f*-electron systems, *Phys. Rev. B* **102**, 134404 (2020).
- [9] J. K. Harada, L. Balhorn, J. Hazi, M. C. Kemei, and R. Seshadri, Magnetodielectric coupling in the ilmenites *MTiO₃* (*M* = Co, Ni), *Phys. Rev. B* **93**, 104404 (2016).
- [10] M. Hoffmann, K. Dey, J. Werner, R. Bag, J. Kaiser, H. Wadepohl, Y. Skourski, M. Abdel-Hafiez, S. Singh, and R. Klingeler, Magnetic phase diagram, magnetoelastic coupling, and Grüneisen scaling in CoTiO₃, *Phys. Rev. B* **104**, 014429 (2021).
- [11] R. Dubrovin, N. Siverin, M. Prosnikov, V. Chernyshev, N. Novikova, P. Christianen, A. Balbashov, and R. Pisarev, Lattice dynamics and spontaneous magnetodielectric effect in ilmenite CoTiO₃, *J. Alloys Compd.* **858**, 157633 (2020).
- [12] S. Zhang, G. Go, K.-J. Lee, and S. K. Kim, SU(3) topology of magnon-phonon hybridization in 2D antiferromagnets, *Phys. Rev. Lett.* **124**, 147204 (2020).
- [13] S. Park and B.-J. Yang, Topological magnetoelastic excitations in noncollinear antiferromagnets, *Phys. Rev. B* **99**, 174435 (2019).
- [14] B. Ma and G. A. Fiete, Antiferromagnetic insulators with tunable magnon-polaron Chern numbers induced by in-plane optical phonons, *Phys. Rev. B* **105**, L100402 (2022).
- [15] D.-Q. To, C. Y. Ameyaw, A. Suresh, S. Bhatt, M. J. H. Ku, M. B. Jungfleisch, J. Q. Xiao, J. M. O. Zide, B. K. Nikolić, and M. F. Doty, Giant spin nernst effect in a two-dimensional antiferromagnet due to magnetoelastic coupling induced gaps and interband transitions between magnonlike bands, *Phys. Rev. B* **108**, 085435 (2023).
- [16] B. Ma, Z. D. Wang, and G. V. Chen, Chiral magneto-phonons with tunable topology in anisotropic quantum magnets, *arXiv:2309.04064*.
- [17] L. Chen, J.-H. Chung, B. Gao, T. Chen, M. B. Stone, A. I. Kolesnikov, Q. Huang, and P. Dai, Topological spin excitations in honeycomb ferromagnet CrI₃, *Phys. Rev. X* **8**, 041028 (2018).
- [18] S. A. Díaz, J. Klinovaja, and D. Loss, Topological magnons and edge states in antiferromagnetic skyrmion crystals, *Phys. Rev. Lett.* **122**, 187203 (2019).
- [19] F. Zhu, L. Zhang, X. Wang, F. J. Dos Santos, J. Song, T. Mueller, K. Schmalzl, W. F. Schmidt, A. Ivanov, J. T. Park *et al.*, Topological magnon insulators in two-dimensional van der Waals ferromagnets CrSiTe₃ and CrGeTe₃: Toward intrinsic gap-tunability, *Sci. Adv.* **7**, eabi7532 (2021).
- [20] See Supplemental Material at <http://link.aps.org/supplemental/10.1103/PhysRevB.110.104419> for magnon Hamiltonian models, Raman spectra of magnons and phonons, quasielastic scattering, Fano resonance of magnon mode, and magnetoelastic effects.
- [21] T. P. Devereaux and R. Hackl, Inelastic light scattering from correlated electrons, *Rev. Mod. Phys.* **79**, 175 (2007).
- [22] M. Ye, E. W. Rosenberg, I. R. Fisher, and G. Blumberg, Lattice dynamics, crystal-field excitations, and quadrupolar fluctuations of YbRu₂Ge₂, *Phys. Rev. B* **99**, 235104 (2019).
- [23] K. Kim, H. Kim, J. Kim, C. Kwon, J. S. Kim, and B. Kim, Direct observation of excitonic instability in Ta₂NiSe₅, *Nat. Commun.* **12**, 1969 (2021).
- [24] G. F. Reiter, Light scattering from energy fluctuations in magnetic insulators, *Phys. Rev. B* **13**, 169 (1976).
- [25] U. Fano, Effects of configuration interaction on intensities and phase shifts, *Phys. Rev.* **124**, 1866 (1961).
- [26] J. Choe, D. Lujan, M. Rodriguez-Vega, Z. Ye, A. Leonardo, J. Quan, T. N. Nunley, L.-J. Chang, S.-F. Lee, J. Yan *et al.*, Electron-phonon and spin-lattice coupling in atomically thin layers of MnBi₂Te₄, *Nano Lett.* **21**, 6139 (2021).
- [27] Y. Tian, M. J. Gray, H. Ji, R. J. Cava, and K. S. Burch, Magnetoelastic coupling in a potential ferromagnetic 2D atomic crystal, *2D Mater.* **3**, 025035 (2016).
- [28] L. Du, J. Tang, Y. Zhao, X. Li, R. Yang, X. Hu, X. Bai, X. Wang, K. Watanabe, T. Taniguchi *et al.*, Lattice dynamics, phonon chirality, and spin-phonon coupling in 2D itinerant ferromagnet Fe₃GeTe₂, *Adv. Funct. Mater.* **29**, 1904734 (2019).
- [29] A. Ghosh, M. Palit, S. Maity, V. Dwij, S. Rana, and S. Datta, Spin-phonon coupling and magnon scattering in few-layer antiferromagnetic FePS₃, *Phys. Rev. B* **103**, 064431 (2021).
- [30] Y. Yamashita and K. Ueda, Spin-driven Jahn-Teller distortion in a pyrochlore system, *Phys. Rev. Lett.* **85**, 4960 (2000).
- [31] O. Tchernyshyov, R. Moessner, and S. L. Sondhi, Order by distortion and string modes in pyrochlore antiferromagnets, *Phys. Rev. Lett.* **88**, 067203 (2002).
- [32] K. Penc, N. Shannon, and H. Shiba, Half-magnetization plateau stabilized by structural distortion in the antiferromagnetic Heisenberg model on a pyrochlore lattice, *Phys. Rev. Lett.* **93**, 197203 (2004).
- [33] L. Savary, K. A. Ross, B. D. Gaulin, J. P. C. Ruff, and L. Balents, Order by quantum disorder in Er₂Ti₂O₇, *Phys. Rev. Lett.* **109**, 167201 (2012).
- [34] C. Kittel, Physical theory of ferromagnetic domains, *Rev. Mod. Phys.* **21**, 541 (1949).
- [35] C. Kittel, Interaction of spin waves and ultrasonic waves in ferromagnetic crystals, *Phys. Rev.* **110**, 836 (1958).
- [36] S. V. Gallego, J. Etxebarria, L. Elcoro, E. S. Tasci, and J. M. Perez-Mato, Automatic calculation of symmetry-adapted

- tensors in magnetic and non-magnetic materials: A new tool of the Bilbao crystallographic server, *Acta Crystallogr. Sect. A: Found. Adv.* **75**, 438 (2019).
- [37] P. Bruno, Magnetic surface anisotropy of cobalt and surface roughness effects within Neel's model, *J. Phys. F: Met. Phys.* **18**, 1291 (1988).
- [38] T. Gutjahr-Löser, D. Sander, and J. Kirschner, Magnetoelastic coupling in Co thin films on W(001), *J. Magn. Magn. Mater.* **220**, 1 (2000).
- [39] A. Balbashov, A. Mukhin, V. Y. Ivanov, L. Iskhakova, and M. Voronchikhina, Electric and magnetic properties of titanium-cobalt-oxide single crystals produced by floating zone melting with light heating, *Low Temp. Phys.* **43**, 965 (2017).
- [40] B. Yuan, E. Horsley, M. B. Stone, N. P. Butch, G. Xu, G.-J. Shu, J. P. Clancy, and Y.-J. Kim, Field-dependent magnons in the honeycomb antiferromagnet CoTiO_3 , *Phys. Rev. B* **109**, 174440 (2024).
- [41] A. Baydin, T. Makihara, N. M. Peraca, and J. Kono, Time-domain terahertz spectroscopy in high magnetic fields, *Front. Optoelectron.* **14**, 110 (2021).
- [42] G. T. Noe, I. Katayama, F. Katsutani, J. J. Allred, J. A. Horowitz, D. M. Sullivan, Q. Zhang, F. Sekiguchi, G. L. Woods, M. C. Hoffmann, H. Nojiri, J. Takeda, and J. Kono, Single-shot terahertz time-domain spectroscopy in pulsed high magnetic fields, *Opt. Express* **24**, 30328 (2016).
- [43] Y. Li, T. T. Mai, M. Karaki, E. V. Jasper, K. F. Garrity, C. Lyon, D. Shaw, T. DeLazzer, A. J. Biacchi, R. L. Dally, D. M. Heligman, J. Gdanski, T. Adel, M. F. Munoz, A. Giovannone, A. Pawbake, C. Faugeras, J. R. Simpson, K. Ross, N. Trivedi, Y. M. Lu, A. R. Hight Walker, and R. Valdes Aguilar, Ring-exchange interaction effects on magnons in the dirac magnet CoTiO_3 , *Phys. Rev. B* **109**, 184436 (2024).
- [44] A. S. Disa, M. Fechner, T. F. Nova, B. Liu, M. Först, D. Prabhakaran, P. G. Radaelli, and A. Cavalleri, Polarizing an antiferromagnet by optical engineering of the crystal field, *Nat. Phys.* **16**, 937 (2020).
- [45] A. de la Torre, D. M. Kennes, M. Claassen, S. Gerber, J. W. McIver, and M. A. Sentef, *Colloquium*: Nonthermal pathways to ultrafast control in quantum materials, *Rev. Mod. Phys.* **93**, 041002 (2021).